Carbon 157 (2020) 525–536

Contents lists available at ScienceDirect

Carbon

journal homepage: www.elsevier.com/locate/carbon

Ripple mediated surface enhanced Raman spectroscopy on graphene

Alisha Prasad [a, 1], Ardalan Chaichi [a, 1], Amirreza Mahigir [c, d], Sushant P. Sahu [a], Deepak Ganta [b], Georgios Veronis [c, d], Manas Ranjan Gartia [a, *]

[a] Department of Mechanical and Industrial Engineering, Louisiana State University, Baton Rouge, LA, 70803, USA
[b] School of Engineering, Texas A&M International University, Laredo, TX, 78041, USA
[c] School of Electrical Engineering and Computer Science, Louisiana State University, Baton Rouge, LA, 70803, USA
[d] Center for Computation and Technology, Louisiana State University, Baton Rouge, LA, 70803, USA

ARTICLE INFO

Article history:
Received 28 July 2019
Received in revised form
8 September 2019
Accepted 25 September 2019
Available online 26 September 2019

Keywords:
Surface-enhanced Raman spectroscopy
Single layer graphene
Rhodamine 6G
Density functional theory
Finite-difference time-domain

ABSTRACT

Surface-enhanced Raman spectroscopy (SERS) has single molecule level bio-chemical detection capabilities. Single layer graphene on SERS substrates shows modest enhancement factor (EF) (~10) primarily from chemical enhancement (CE) mechanism. Improvement in EF will have significant impact on applications of graphene in optoelectronics. This limitation is caused by poor interaction of visible light at near infrared frequencies with graphene monolayers. We report an assembly of single-layer graphene (SLG) on a three-dimensional (3D) Au@Ag, core-shell structure that enhances light-matter interactions and modulates light absorption in graphene due to formation of graphene ripples. We demonstrate a SERS EF of ~1,000 using 633 nm excitation laser with the designed SLG/SERS substrate. The Raman scattering cross-section of R6G molecule was found to be enhanced by a factor of ~10^2–10^3, and limit of detection obtained was 100 pM using the SERS substrate. The enhancement is primarily due to increase in polarizability and anisotropy from rippled graphene substrate. The finite-difference-time-domain electromagnetic simulation showed enhancement of local electromagnetic field leading to enhanced excitation of the molecule. Density functional theory based quantum mechanical simulation studies showed the charge transfer from graphene-to-R6G molecule, leading to enhanced emission of Raman scattering.

1. Introduction

Due to surface-enhanced Raman spectroscopy (SERS)'s ability to detect the chemical fingerprint of molecules at the single molecule level, SERS has been employed in numerous biochemical sensing applications [1]. For example, gold nanoparticles encapsulated with carbon shell and surface modified with DNA, have been utilized for SERS applications to detect trace amount of water contamination [2]. Electromagnetic ($G_{EM} \sim 10^6$ -10^{10}) and chemical ($G_{CM} \sim 10^2$) enhancement mechanisms contribute to the overall enhancement associated with SERS [3–5], where G is the enhancement factor. Increase in the intensity of the local electromagnetic field due to resonance excitation of localized surface plasmons is the foundation of electromagnetic enhancement mechanism (EM) [6]. This mechanism is directly related to the field enhancement factor ($G = |E/E_0|^4$), where E_0 is the incident electromagnetic field, and E is the enhanced field in presence of surface plasmon resonance excitation [7,8]. As a result, the enhanced Raman signal depends on the overlap between the excitation wavelength during Raman scattering and the plasmon resonance wavelength of the substrate [9,10]. In addition, the chemical enhancement mechanism is mainly dominated by substrate/molecule interactions. In chemical enhancement mechanism (CM), the electronic structure of molecules can dramatically affect the value of maximum enhancement obtained at a particular excitation wavelength [11,12]. However, since CM and EM enhancement mechanisms can occur simultaneously, it is not easy to discern these two mechanisms in the analysis of SERS systems.

Single layer graphene (SLG) is the thinnest known allotrope of carbon. It possesses some unique optoelectronic properties that can be beneficial in the amplification of the SERS process [13–16]. So far graphene has been utilized as a Raman probe [17], SERS probe [18,19], fluorescence quencher to improve the Raman scattering efficiency [20], and as a way to intensify the chemical enhancement

* Corresponding author.
E-mail address: mgartia@lsu.edu (M.R. Gartia).
[1] Equal contribution.

https://doi.org/10.1016/j.carbon.2019.09.078
0008-6223/

mechanism [21]. In addition, graphene hybrid structures have been utilized to improve the performance of SERS substrates by acting as a single layer spacer for metal-molecule isolation [22], as a molecule catcher (utilizing sticking properties of graphene like strong π-π stacking interactions with aromatic molecules containing benzene rings) [23], as an atomically flat surface on SERS substrate to improve reproducibility [24], as a passivation layer for preventing oxidation [25], and as a conformable layer on flexible substrates [24,26,27]. However, the enhancement factors obtained from graphene SERS substrates are limited to less than 100 [21,28]. By utilizing various architectures of plasmonic Au nanoparticles (NPs) along with 3D crumpled graphene structure, a further improvement in the SERS enhancement factor of ~10–30 was observed in reference to flat graphene-Au NPs [27,29]. Similarly, 3D architectures such as crumpled graphene with nanoparticles [27], multilayer graphene with nanoparticles [26], and graphene-Au pyramid structures [30] were realized. However, the enhancement factor obtained with graphene layer compared to the absence of graphene layer was modest (~10). Since the surface plasmon of graphene is in the terahertz range [31], EM contribution from graphene is not expected for visible laser excitation. The enhancement mechanism on graphene is therefore primarily due to CM. In a recent study, researchers probed the CM mechanism using a silicon electrode coated with gold nanoparticles covered multilayer graphene and quantum dots structure [32].

Integrating graphene with plasmonic nanostructures also stems from the desire to enhance light-matter interactions. Graphene is a promising material for many optoelectronic applications [33] such as ultrafast photodetectors [34], modulators [35], and lasers [36]. Due to the two-dimensional structure of graphene, electrons move throughout a single layer graphene sheet in a massless fermions manner with considerably high charge transfer and mobility [37–39]. However, the interaction of light with graphene is weak with each layer of graphene absorbing light corresponding to the fine structure constant (~2.3% of light in the visible range per layer). This is a significant limitation for the utilization of graphene in many optoelectronic applications at near infrared and visible frequencies. One of the ways to enhance light-matter interactions is to integrate graphene with plasmonic structures to manipulate light absorption in graphene. Recently, a research group created a heterostructured SERS substrate composed of free-standing Si nanowires and surface-decorated with Au/graphene NPs, for SERS-based chemical sensing [40].

In this paper, we introduce a single-layer graphene on a 3D Au@Ag (Ag coated Au nanopillar) core-shell structure to study the ripple mediated SERS enhancement properties of graphene. Experimental and computational results demonstrate an enhancement factor of ~1,000 on the 3D rippled structure compared to a planar graphene structure. The EM mechanism is investigated using finite-difference time-domain (FDTD) simulations, while the CM mechanism is investigated using density functional theory (DFT) simulations.

2. Experimental procedure

2.1. Sample preparation

2.1.1. Synthesis of Au@Ag core shell nanopillars over the silicon wafer

A four-inch p-type doped single crystalline silicon wafer was used as the substrate with resistivity and crystalline orientation of 0.2–0.5 Ω cm^{-1} and (1, 0, 0), respectively. Deionized water, acetone and isopropyl alcohol were used for cleaning the substrate. For better adhesion, the original oxide layer was kept intact on the substrate. Prior to thermal dewetting process, e-beam evaporation was utilized to deposit Au layer with a thickness of 6 nm. In order to induce thermal disturbance into gold thin layer, a Jipelec rapid thermal processor (RTP) was utilized. The heating time remarkably decreases by utilizing the RTP system and the whole process can be accomplished in about 5 min. Temperature range of 100–500 °C was selected for 90 s accompanied by nitrogen gas purge into the chamber to prevent further oxidation. Afterwards, dry etching using ICP-RIE (inductively coupled plasma reactive ion etching) followed by STS (Surface Technology System) was performed. The continuous process of etching (by SF_6 and O_2) and passivation (by C_4F_8) results in a high aspect ratio structure under the pressure of about 100 mTorr with RF powers of 12 and 600 W for the capacitive chamber and inductive chamber, respectively. CHA SEC-600 electron-beam evaporator (10 kV) was utilized for Ag deposition under the pressure of 10^{-7} mTorr and evaporation rate of 0.5 Å s^{-1}. To determine the optimum thickness of SERS performance, deposition process was accomplished for thicknesses ranging between 20 and 140 nm.

2.1.2. Deposition of single-layer graphene over the nanopillar surface

Chemical Vapour Deposition (CVD) was employed for synthesizing single layer graphene on two sides of a copper substrate. Afterwards, one side of the sample was protected by deposition of Polymethyl Methacrylate (PMMA). The other side was exposed to O_2 plasma and $FeCl_3$ solution for etching process. The protected side (graphene/PMMA) was transferred to the prepared plasmonic structure by wet transferring method. A solution of methanol and dichloromethane was used to dissolve the PMMA layer.

2.1.3. Deposition of R6G over graphene covered plasmon supporting SERS substrate

We utilized two different methods to deposit the Rhodamine 6G (R6G) on the surface of the nanopillars in order to avoid the formation of aggregates. (1) Spin-coating (100 rpm), and (2) Drop-coating. For spin-coating, the solution was placed onto the SERS substrate and rotated at a speed of 100 rpm, while in drop-coating few drops of the solution were simply placed onto the surface of the SERS substrate and heated at a temperature of ~60 °C to quickly evaporate the water without having the “coffee-ring” effect. Both are evaporation-driven deposition processes and have been widely used by researchers in similar studies [41,42].

2.2. Characterization

For Raman spectra studies, Renishaw Raman microscope/spectroscope (at magnification 20X) was utilized. Laser excitation of $\lambda = 633$ nm was utilized with an exposure time of 10 s in the wavenumber range of 200–3000 cm^{-1}. Quanta 3D Dual Beam FEG FIBSEM was used for acquiring the scanning electron micrographs to confirm each step of sample preparation. FIB was also employed during SEM imaging to perform cross-sectional studies of these samples. For Raman maps, StreamHR image acquisition mapping was chosen with an objective lens of 50X, an excitation laser wavelength of 633 nm and 532 nm (power of 100% for both), grating of 1200 l/mm (633/780), and integration time of 0.01 s, in the wavenumber range of 200–2000 cm^{-1}, with static mode centered around 1500 cm^{-1}.

2.3. Simulation

The 3D FDTD (Lumerical Solutions Inc. Software) method was used to calculate the field enhancement and field profiles. The distribution of electric field on the graphene coated plasmonic nanopillar arrays was also calculated using the FDTD software. To

numerically resolve the monolayer of graphene (thickness = 0.34 nm), we implemented a mesh size of 0.1 nm. To optimize the computational time, we used a mesh size of 1 nm for the rest of the regions in the simulation system. The ε value (dielectric permittivity) for Ag and Au was obtained from CRC data [43]. We simulated graphene as a 3D anisotropic layer with a complex refractive index having variation defined by: $n = 3 + \frac{j5.446\lambda}{3}\ \mu m^{-1}$ [44]. To check the validity of this model, we first calculated the absorption in the bare monolayer graphene (suspended in air) and obtained a value close to ~2.3% in the visible-NIR wavelength ranges [45]. To obtain the electromagnetic field distributions on the graphene coated plasmonic structure, periodic boundaries (x, y), and perfectly matched layer (PML) absorbing boundaries (z) were used [46]. A plane wave excitation light (broadband, x-polarized) was utilized as excitation source. The electronic energy levels, vibrational spectra, and charge transfer mechanism of R6G were investigated using DFT. Quantum chemistry code (Gaussian-09) with 6−31 G basis set and B3LYP density functional were utilized in the simulation. An integration accuracy of 4 and convergence accuracy of 10^{-8} were selected during the calculation.

3. Results and discussion

3.1. Characterization of the rippled SLG/SERS substrate

The 3D schematic in Fig. 1a shows the Au@Ag core shell nanopillars over the silicon wafer where a single-layer graphene spreads over the nanopillar surface creating ripples to form a plasmon supporting SERS substrate.

The proficiency of the designed SERS substrate was identified by analyzing Raman spectra of dye molecules such as R6G as a Raman reporter. Fig. 1b shows the SEM (Scanning Electron Micrographs) image of graphene on the SERS substrate whereas Fig. 1c, d shows the optical image. R6G appears as yellow in the optical image (shown with the blue arrows in Fig. 1d). The cross-sectional SEM image from this optical image (highlighted black square region) is shown in Fig. 1e. In addition, FIB (Focused Ion Beam) was also employed during SEM imaging to obtain the cross-sectional interpretation of the SERS substrate. Fig. 1f is a SEM image showing graphene over the 10 μm × 10 μm area of the substrate, while Fig. 1g shows the FIB cut area showing the cross-sectional view of graphene, Ag coated Au nanopillars, and silicon substrate. According to literature reports, R6G molecules are conjugated through the $-NH_2$ group (amino groups) to the single layer graphene by physisorption process [47].

The optical properties in Fig. 2, confirmed the growth of SLG by CVD - process. The transmission spectra in Fig. 2a show that only ~2.3% of the incident light was absorbed, which is a characteristic of SLG's unique electronic structure, and are similar to results presented by Nair et al. [48]. In order to investigate the peaks at ~600 nm and ~640 nm, we also ran a FDTD simulation to calculate the light transmission through the SLG on a glass, and after removing the graphene layer (just through glass) from 400 to 800 nm, respectively (Supplementary Figure S1). The transmission was flat and no peaks showed up, meaning that the peaks are not originating from graphene and they are coming from the absorption at the glass substrate [49].

The main objective of the present study was to create a rippled surface by laying graphene on the Au@Ag core shell nanopillars, and utilize it as a SERS substrate. To better understand the SERS substrate activity, we evaluated the optical scattering and reflectance properties as shown in Figs. 2b and c. A reflection spectral peak at 671 nm was found for the Au@Ag core shell nanopillars on the SiO_2 substrate with graphene (orange line, Fig. 2c). A broader peak at 668 nm was observed for the nanopillars without graphene (blue line, Fig. 2c). The 2% difference (or 3 nm peak shift) in the relative reflection with and without graphene might be due to peak broadening originating from the coupling between localized surface plasmons (LSPRs) of the nanopillars and graphene. In a similar study on graphene covered plasmonic nanoparticles to study the SERS effect, the relative reflectance spectra peak for the graphene/AuNPs was found at ~606 nm [14]. The near resonance wavelength of the graphene covered Au@Ag core shell nanopillars, gives an advantage of utilizing the 633 nm laser for Resonance Raman spectroscopy, to yield stronger SERS activity [50]. Fig. 2b also showed a 3% difference (or 12 nm peak shift) in scattering from the graphene covered Au@Ag core shell nanopillars in comparison to bare nanopillars. This might originate from the ripples which are formed on the surface of graphene. Due to the non-horizontal orientation of graphene plane, the absorbed light is reemitted at various angles by induced polarization. Additionally, the scattering phenomenon in this system is affected by the waveguiding ability of graphene [51,52].

3.2. Measurement of Raman spectra on the rippled SLG/SERS substrate

The Raman spectra of the rippled SLG/SERS substrate was studied by choosing the 633 nm excitation laser to overlap with the LSPRs of the plasmonic Au@Ag core shell-nanopillars coupled with

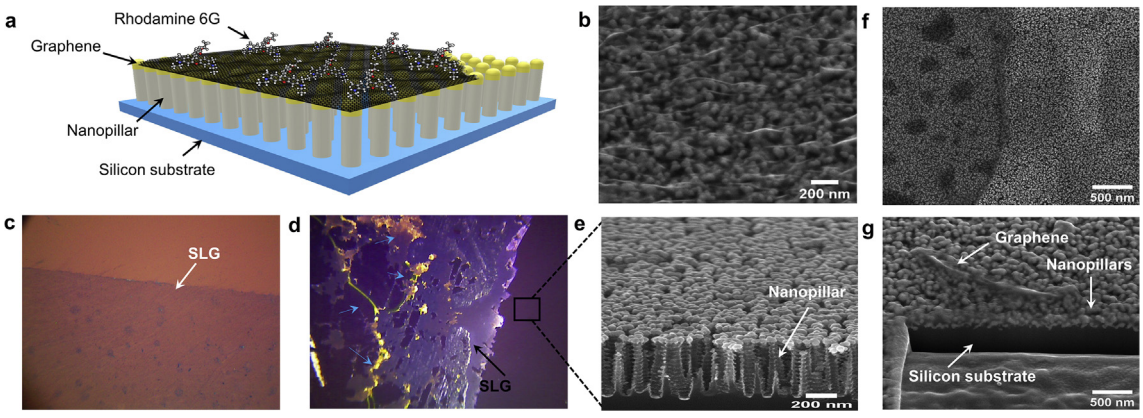

Fig. 1. (a) Schematic diagram showing graphene ripple on the plasmonic nanopillar SERS substrate. (b) Scanning Electron Micrographs (SEM) of graphene on the SERS substrate. (c, d) Optical image of graphene on the SERS substrate. Rhodamine 6G (R6G) is appearing as yellow in the image (shown by blue arrows). (e) Vertical cross-sectional SEM image of the Au@Ag core-shell nanopillars taken from the black square region of image shown in (d). (f) SEM image showing graphene over the 10 μm × 10 μm area of the substrate. (g) Focused Ion Beam (FIB) cut area showing the cross-sectional view of graphene, Ag coated Au nanopillar, and silicon substrate. (A colour version of this figure can be viewed online.)

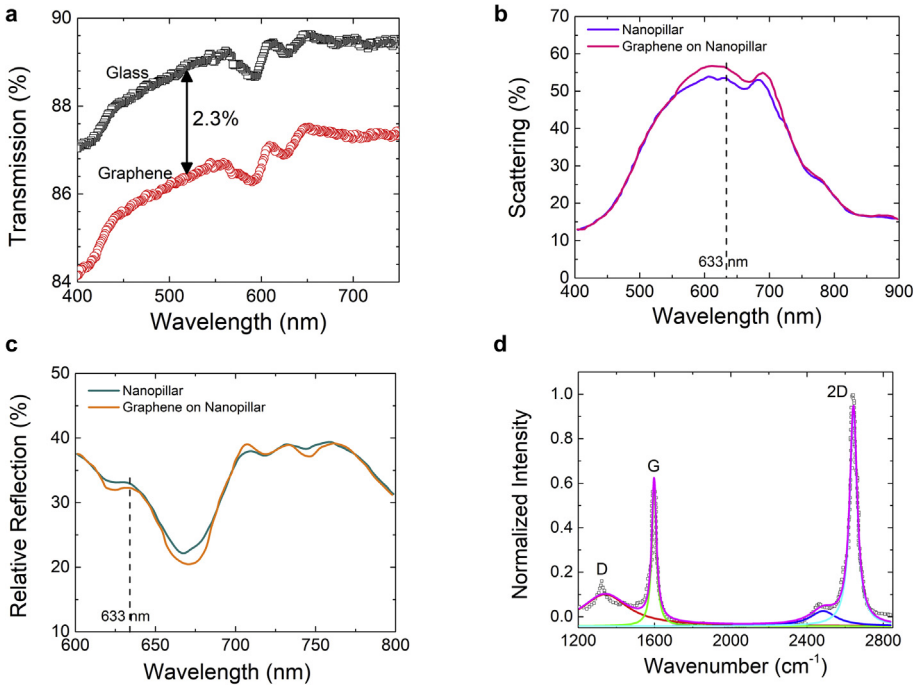

Fig. 2. Optical properties of graphene covered Au@Ag core-shell nanopillars SERS substrate. (a) Transmission spectra. (b) Scattering spectra. (c) Reflection spectra. (d) Measured Raman spectra of the single-layer of graphene on the SERS substrate. The Lorentzian fits of the full spectra (pink line) and the corresponding fit to individual D (red), G (green) and 2D (cyan) bands are shown. (A colour version of this figure can be viewed online.)

graphene system. The typical Raman spectra of graphene has three signature peaks namely, the D-peak (1318 cm^{-1}), 2D-peak (2628 cm^{-1}), and G-peak (1580 cm^{-1}) [53,54] (Fig. 2d). These results again confirm the presence of SLG on our substrate. Additionally, the intensity of the G and 2D bands were higher in comparison to the one of the D band. The presence of SLG was further confirmed by performing deconvolution of the peaks in Fig. 2d. The FWHM of the peaks were evaluated by fitting Lorentzian functions to the peaks; the 2D/G ratio was also calculated. Supplementary Figure S2 shows that the 2D/G ratio was above 2 and below 6, which is a characteristic of monolayer graphene [55,56]. In addition, the FWHM in Figure S3 was found to be in the range of 15–20 cm^{-1} which further confirms that the synthesized graphene is a SLG [57,58]. After confirming the presence of SLG, the SERS activity of the designed graphene covered plasmonic substrates was measured.

As shown in Fig. 3a, the Raman spectra was acquired for dye R6G molecules adsorbed on the graphene covered substrate (blue line) after casting 1 nM solution of R6G, and compared with bulk R6G (red line) with a concentration of 1 μM in solution phase, and bulk graphene coated on a flat surface (black line). The results showed the three unique peaks of SLG in all the acquired Raman spectrum with graphene. Also, the R6G peaks observed at 1650 & 1511 cm^{-1} due to aromatic C–C stretching, 1184 cm^{-1} from C–O–C stretch, and 773 cm^{-1} from aromatic C–H bending are in accordance with previous literature reports [59]. A Si peak from the SiO_2/Si substrate at 520 cm^{-1} was also observed [60]. The vibrational modes of the peaks are tabulated in Table S1.

The ripples created from the graphene covered plasmonic SERS substrate provided >1000× higher SERS enhancement factor (EF) for each identified Raman peak in comparison to the flat substrate acquired under the same conditions as seen in Fig. 3b and as summarized in Table S2. The experimental SERS EF for this SERS system was calculated by the following relationship, $EF = \frac{I_{(Rippled)SERS} \times N_{(flat)bulk}}{I_{(flat)bulk} \times N_{(rippled)SERS}}$, where $I_{(Rippled)SERS}$ and $I_{(flat)bulk}$ are defined as the SERS intensities obtained from all the Raman bands presented in Fig. 3a and assigned for different stretching modes of SLG and R6G on the flat and rippled substrate, respectively. $N_{(flat)bulk} = n_{(flat)bulk} \times N_A = C_{(flat)bulk} \times V_{(flat)bulk} \times N_A$ is defined as the number of molecules in the bulk solution utilized in Raman measurement on the flat surface. $N_{(rippled)SERS} = n_{(rippled)SERS} \times N_A = C_{(rippled)SERS} \times V_{(rippled)SERS} \times N_A$ is defined as the number of molecules on the rippled surface. Here, $n_{(flat)bulk}$and $n_{(rippled)SERS}$ are the number of R6G molecules in the scattering volume; $V_{(flat)bulk}$and $V_{(rippled)SERS}$ are the scattering volumes (same volume of droplet was dropped to keep the scattering volume constant, so $V_{(flat)bulk} = V_{(rippled)SERS}$); $C_{(flat)bulk}$ and $C_{(rippled)SERS}$ are the R6G concentrations. For our experiment, $C_{(flat)bulk}$ = 100 μM, $C_{(rippled)SERS}$ = 100 nM, and the estimated EF was found to be ~10^3. The rippled graphene system showed a maximum EF of 6.9 × 10^3 observed at the 1511 cm^{-1} vibrational mode of the R6G molecule (Table S2) at an excitation wavelength of 633 nm.

We also evaluated the concentration dependent SERS spectra of R6G on the graphene covered Au@Ag core-shell substrate at concentration ranges of 10 pM–100 nM. In Fig. 3c we observe that a minimum of 100 pM concentration is required to see distinguishable Raman signals. The variation of SERS intensity with concentration at the 1511 cm^{-1} Raman peak is shown in Fig. 3d. The limit of detection was found to be 100 pM.

For visual presentation, we also acquired the Raman maps, and their corresponding spectra as seen from Fig. 4, from both graphene on flat and graphene on nano substrate. A clear difference can be observed with and without graphene, in both bright field images (Figs. 4a, g) as well as Raman maps (Figs. 4b, c,h,i) (without graphene (blue), with graphene (green)). The Raman maps are pseudo colored based on the intensity. The peak at 521 cm^{-1} corresponds to Si, and the peak at 959 cm^{-1} corresponds to Si–OH (Figs. 4d, j).

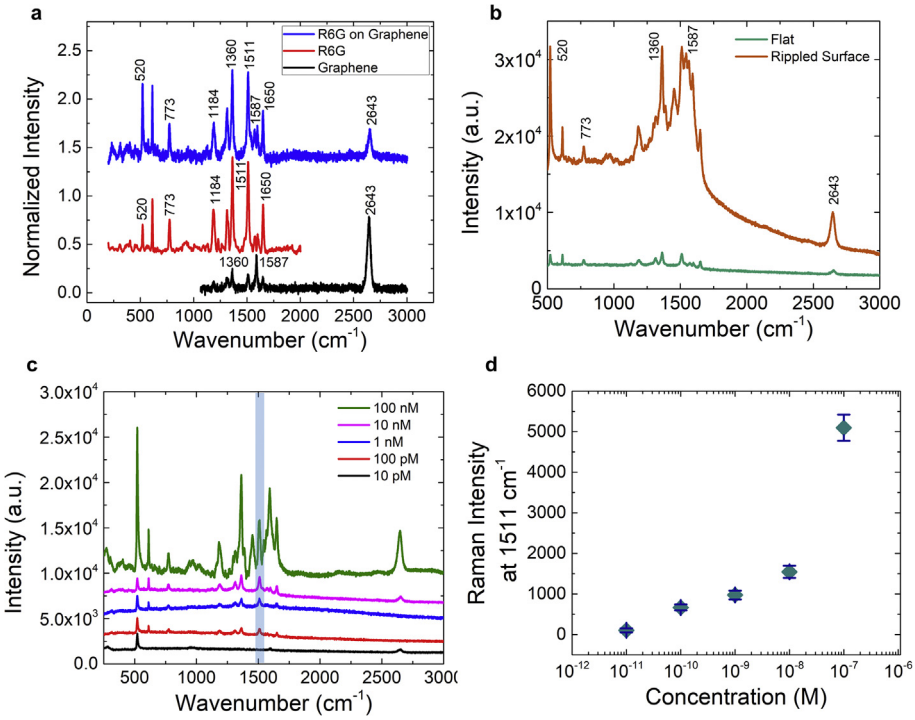

Fig. 3. (a) Raman spectra of R6G on graphene coated nanostructured SERS substrate (blue line (100 nM)), bulk R6G (red line (1 μM)) and single layer graphene on flat surface (black line). (b) Evaluation of enhancement factor from surface enhanced Raman spectroscopy (SERS) substrate in comparison to flat surface. The corresponding concentrations are $C_{(flat)bulk} = 100$ μM and $C_{(rippled)SERS} = 100$ nM. (c) SERS spectra of R6G on the Au@Ag core-shell substrate at concentrations ranging from 10 pM to 100 nM. (d) SERS intensity as a function of concentration at the 1511 cm^{-1} Raman peak. (A colour version of this figure can be viewed online.)

The other two peaks at 1327 and 1587 cm^{-1} corresponds to the D and G peak of the graphene, respectively (Figs. 4e, k). The Raman mapping results also showed the uniformity of the SERS substrate. The SERS enhancement is evident from the comparison of Fig. 4f and l. Furthermore, Fig. 4, wherein the number of acquired spectra are in the range of 10,000–25,000 within an area of 300 μm × 300 μm, demonstrates the reproducibility within a sample. The reproducibility among samples was shown by plotting the average SERS intensity at 1587 cm^{-1} with standard deviation for three different substrates as shown in Supplementary Figure S4.

The cross-section of R6G for the Raman scattering on graphene covered Au@Ag core-shell substrate was calculated using the relationship [61] $\sigma_{R6G} = \frac{\sigma_G I_{R6G} C_G}{I_G C_{R6G}}$, where σ_G is the cross-section of graphene for the Raman scattering, C_{R6G} is the R6G concentration, C_G is the concentration of graphene, I_{R6G} is the Raman peak intensity of R6G, and I_G is the Raman peak intensity of graphene. The quantity $\sigma_G C_G$ was found to be ~ $0.9 - 5.4 \times 10^{-11}$ Sr^{-1}[61–63]. In Fig. 5a, the intensities of the Raman peaks of R6G and graphene were calculated by measuring the area under the peaks at 1650 cm^{-1} and 1572 cm^{-1}, respectively. Accordingly, $I_G = 5.8$, and $I_{R6G} = 10.5$. Here, we used 100 nM concentration of R6G and utilized 1 μL of sample to obtain the Raman spectra. The corresponding number of molecules of R6G on the surface will be $C_{R6G} = 6.023 \times 10^{10}$. With these quantities, the cross-section of R6G for the Raman scattering process on the graphene coated SERS is found to be $\sigma_{R6G} = 0.27 - 1.62 \times 10^{-21}$ $cm^2 \cdot Sr^{-1} \cdot molecule^{-1}$. Shim et al. [64] measured the cross-section of R6G for the Raman scattering in solution to be 2.0×10^{-23} $cm^2 \cdot Sr^{-1}$ per molecule. Hence, the increase in the cross-section of R6G for the Raman scattering on graphene covered Au@Ag core-shell substrate is ~10^2–10^3, which is about the same order of magnitude as our SERS enhancement factor.

We provide another evidence of the rippled structure of graphene in Figs. 5b–e. Fig. 5b shows the comparison of the G peak of graphene on a flat surface (unstrained) and on the SERS substrate (strained). The G peak of unstrained graphene appeared as a single peak at 1587 cm^{-1}, whereas the G peak of strained graphene split into two peaks at 1572 and 1598 cm^{-1}. The split in G peak is a sign of shear strain [65,66]. Interestingly, the 2D peak of graphene on the SERS substrate was red shifted compared to the graphene on flat substrate (Figs. 5c–e), which is due to the combined effect of charge transfer from the plasmonic substrate [67] and the strain caused by the ripple structure.

3.3. SERS enhancement mechanism

Here, we investigate the electromagnetic and chemical SERS enhancement mechanisms on the designed SLG/SERS substrate.

3.3.1. Electromagnetic (EM) enhancement mechanism

The EM enhancement occurs at the interface between the Au@Ag core-shell nanopillars because of the local electromagnetic 'hot spots' associated with the resonance excitation of LSPRs. In order to understand the effect at the interface between the SLG and the nanopillar arrays, we set periodic boundary conditions along the *x* and *y* axis. Fig. 6a shows the 3D schematic of the simulated structure. A nanopillar array with 30 nm lattice constant on silicon substrate supports the core-shell Au@Ag nanoparticles which are covered with a monolayer of rippled graphene. Figs. 6b–d show the 3D normalized electric field intensity distribution in a few unit cells of the structure, at an excitation wavelength of 633 nm, as well as at Raman emission wavelengths of rippled graphene, at 703 nm and 760 nm, respectively. The plasmonic nanostructures enhance the localization of the field in the vicinity of the graphene monolayer, enhancing the optical absorption rate in the graphene. Figs. 6e–g

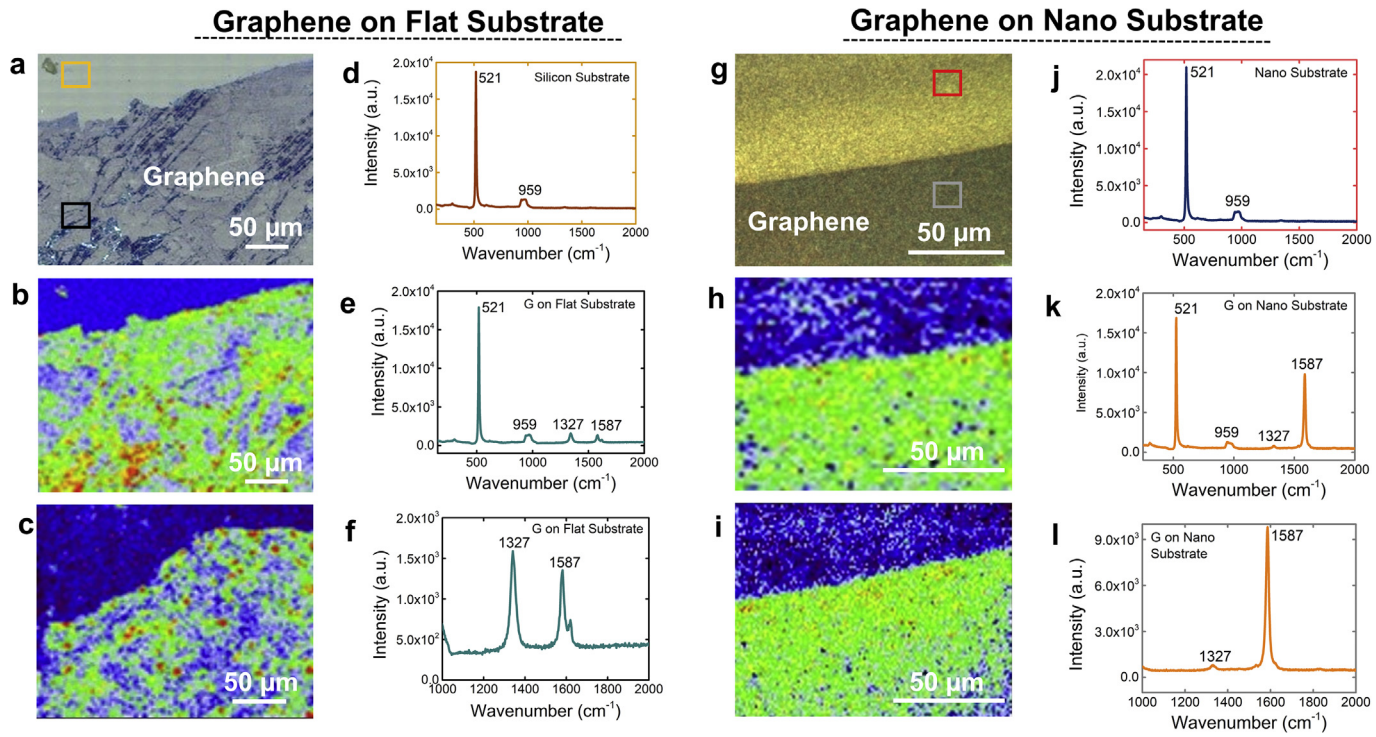

Fig. 4. Representative bright field images of (a) graphene on flat substrate, and (g) graphene on nanostructured substrate. Raman mapping of graphene on flat substrate (b) using 532 nm laser excitation; magnification: 50X; number of acquired spectra: 25017), and (c) using 633 nm laser excitation; magnification: 50X; number of acquired spectra: 14012). Raman spectra on (d) silicon substrate (orange square highlighted area shown at the inset of (a)), (e) graphene on flat substrate (black square highlighted area shown at the inset of (a)), (f) zoomed in spectral region from 1000 to 2000 cm^{-1} shown in Fig. 4e. Raman mapping of graphene on nano substrate (h) using 532 nm laser excitation; magnification: 50X; number of acquired spectra: 10850), and (i) using 633 nm laser excitation; magnification: 50X; number of acquired spectra: 10850). Raman spectra on (j) nano substrate (red square highlighted area shown at the inset of (g)), (k) graphene on nano substrate (black square highlighted area shown at the inset of (g)), (l) zoomed in spectral region from 1000 to 2000 cm^{-1} shown in Fig. 4k. (A colour version of this figure can be viewed online.)

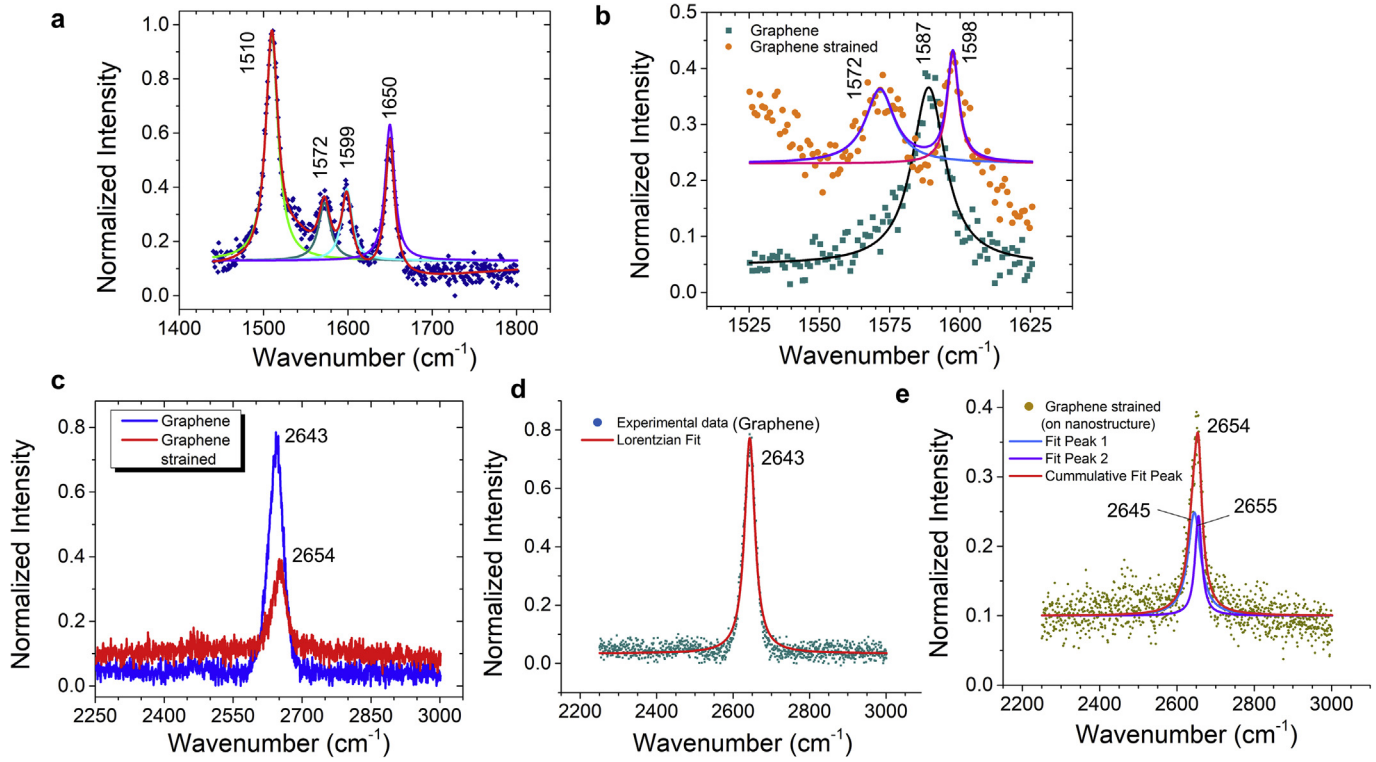

Fig. 5. Raman spectra of R6G on graphene coated nanostructured substrate showing the (a) experimental data (blue diamonds), and Lorentzian fits. The overall fit is shown with the red line. (b) Comparison of G peak for unstrained graphene (on flat surface) and strained graphene (on nanostructured surface leading to ripple). The splitting of G peak shows that graphene is under strain on the nanostructured surface. (c) Comparison of 2D peak for unstrained graphene (blue line) and strained graphene. The corresponding Lorentzian fits to the experimental data are shown in (d) for unstrained graphene, and in (e) for strained graphene. The red shift of the graphene 2D peak is due to the charge transfer and the strain due to the ripple effect. (A colour version of this figure can be viewed online.)

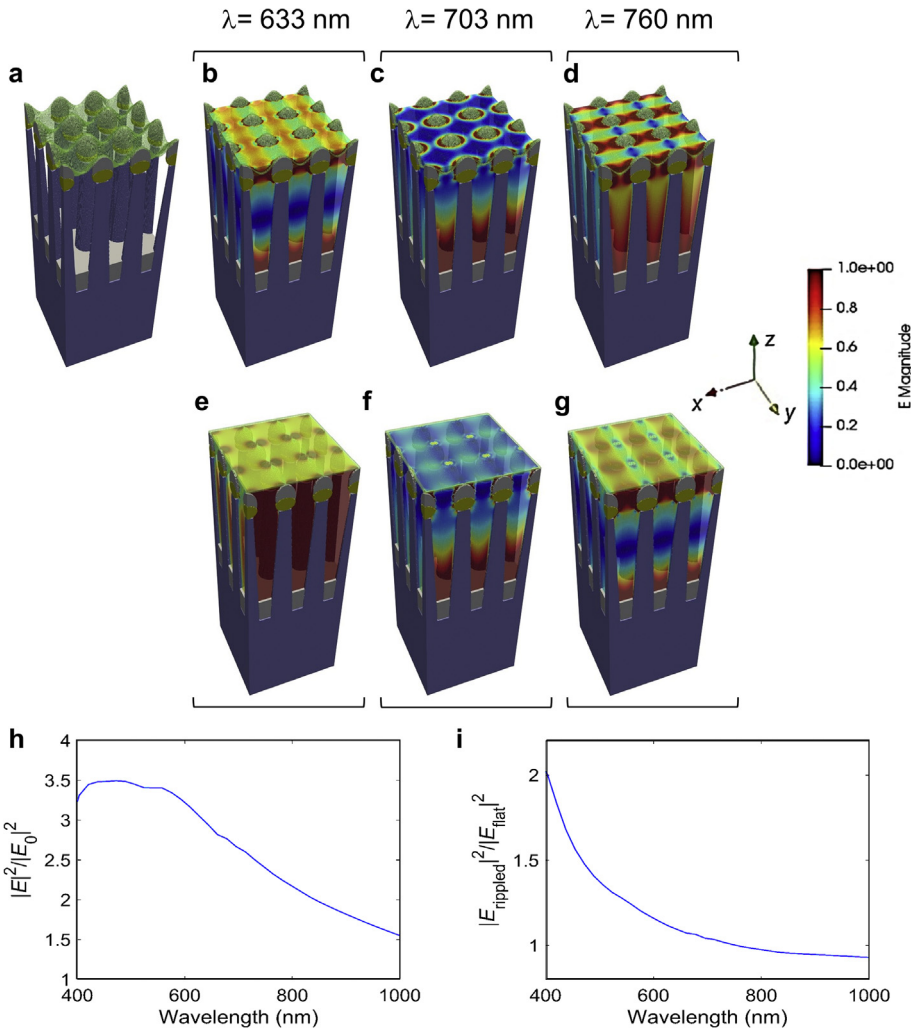

Fig. 6. (a) Schematic of rippled graphene (SLG) on the core-shell Au@Ag nanopillars structure; Electromagnetic field distribution for (b, c, and d) rippled graphene on nanopillar substrate; (e, f, and g) flat graphene on nanopillar substrate; (h) variation of electromagnetic field enhancement with wavelength on rippled graphene coated nanopillar with respect to incident field; (i) variation of electromagnetic field enhancement with wavelength on rippled graphene coated nanopillar with respect to flat graphene coated nanopillar. (A colour version of this figure can be viewed online.)

show the 3D normalized electric field intensity distribution for the flat surface.

3D FDTD simulations were performed to calculate the local electromagnetic field at the interface of rippled graphene and the nanopillar array. Fig. 6h shows an enhancement of ~3× in the electric field intensity compared to the incident field (λ = 633 nm) as a function of wavelength.

The electric field was calculated for normal incidence of excitation (E_0) and was averaged over the surface of the rippled graphene monolayer. Fig. 6i compares the field enhancement achieved by the rippled graphene surface compared to flat graphene surface on the same plasmonic nanopillar array substrate. The results show that the enhancement in field intensity at the rippled graphene is higher at shorter wavelengths (λ < 600 nm) compared to longer wavelengths (λ > 800 nm). This is expected since at longer wavelengths the fields are more scattered in the surrounding media, so a flat graphene would experience higher field. But at shorter wavelengths the fields are more confined between the metallic nanostructures, and a rippled graphene would experience higher field. The electric field distribution with and without graphene on the metal coated nanopillar substrate at the G and 2D bands corresponding to SLG was also calculated (Supplementary Figure S5).

3.3.2. Chemical (CM) enhancement mechanism

The EM enhancement of graphene covered structures has been widely reported [1,24,26,30,68,69] but the CM enhancement of graphene conjugated molecules is less explored [70–72]. In the present study, we focused on highlighting the charge-transfer enhancement originating from the metal–molecule conjugate by investigating the electronic and vibrational properties of a probe molecule R6G by DFT studies.

Fig. 7a shows the optimized geometry of graphene using DFT, with high electron density along the zig-zag (trans) edge compared to arm chair (cis) which is confirmed by existing experimental reports using AFM (Atomic Force Microscopy) [73,74] and STM (Scanning Tunneling Microscopy) [75], respectively. Another evidence for the feasibility of using limited size graphene sheet can be seen from Fig. 7c.

The graphene simulated here has a bandgap due to its finite size. The bandgap decreases (or vanishes) with increase in graphene layers/sheets [76,77]. From Fig. 7b, it can be inferred that charge

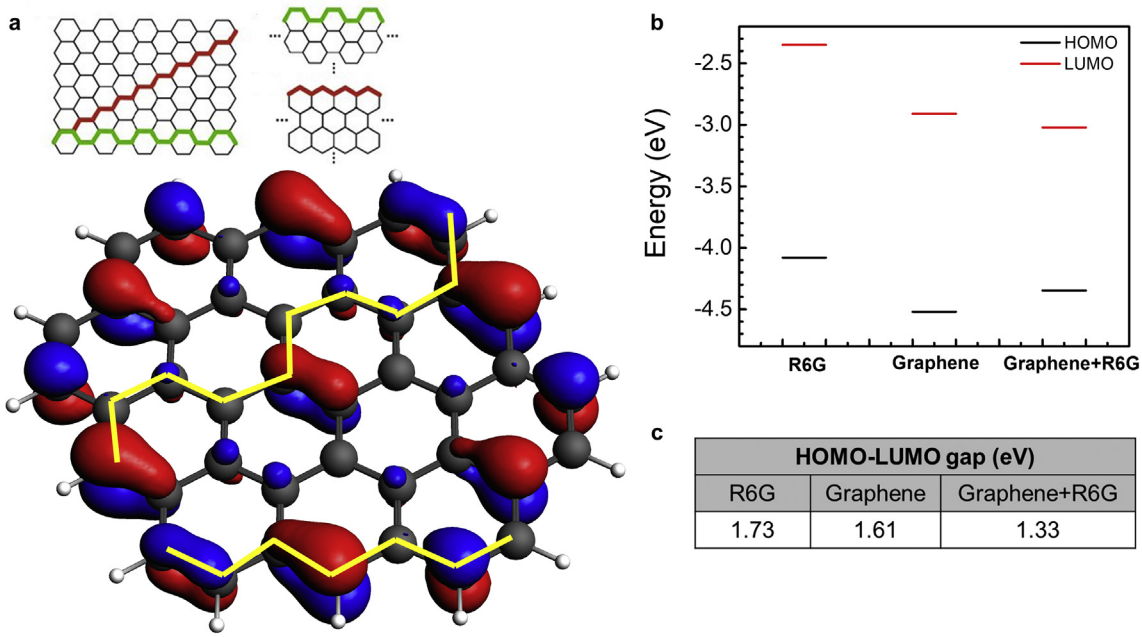

HOMO-LUMO gap (eV)		
R6G	Graphene	Graphene+R6G
1.73	1.61	1.33

Fig. 7. (a) Optimized geometry of graphene using Density Functional Theory (DFT). High electron density along the zig-zag (trans) edge compared to arm chair (cis) is shown. The inset shows the schematic of the arm chair (green) and zig-zag (red) configuration of graphene edge. (b) Position of HOMO and LUMO energy level and (c) HOMO-LUMO band gap for R6G, Graphene and R6G conjugated graphene. (A colour version of this figure can be viewed online.)

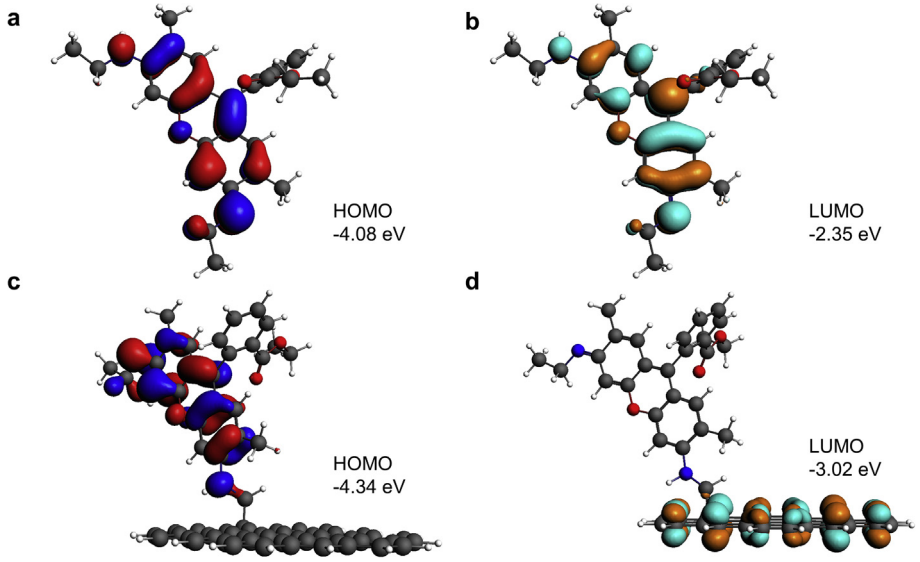

Fig. 8. Electron density plot showing the (a) HOMO and (b) LUMO level for R6G before adsorption to graphene. Electron density plot showing the (c) HOMO and (d) LUMO level for R6G after adsorption to graphene. (A colour version of this figure can be viewed online.)

transfer is possible from the LUMO (lowest unoccupied molecular orbital) of graphene to the HOMO (highest occupied molecular orbital) of R6G as the LUMO is at higher energy. The HOMO of graphene is lower than that of an isolated R6G molecule leading to excited electrons in the LUMO of graphene dropping to the HOMO of R6G, rather than its own HOMO. The HOMO-LUMO gap of isolated R6G is 1.73 eV. The HOMO level of R6G is close to the Fermi energy of graphene (~−4.6 eV). Thus, strong interaction between R6G and graphene is possible and the orbital energy and electron density of R6G is modified due to the presence of graphene. The LUMO of the hybrid structure is significantly lowered from −2.35 eV to −3.02 eV. The decrease in bandgap leads to more efficient Raman excitation.

Furthermore, we also show the electron density plot showing the HOMO and LUMO level for both before (Figs. 8a and b) and after (Figs. 8c and d) adsorption of R6G to graphene. The HOMO and LUMO for R6G before adsorption were −4.08 eV and −2.35 eV, respectively, while after adsorption of R6G to graphene they reduced to −4.34 eV and −3.02 eV, respectively. From these results, it is evident that the HOMO of R6G becomes more negative in the

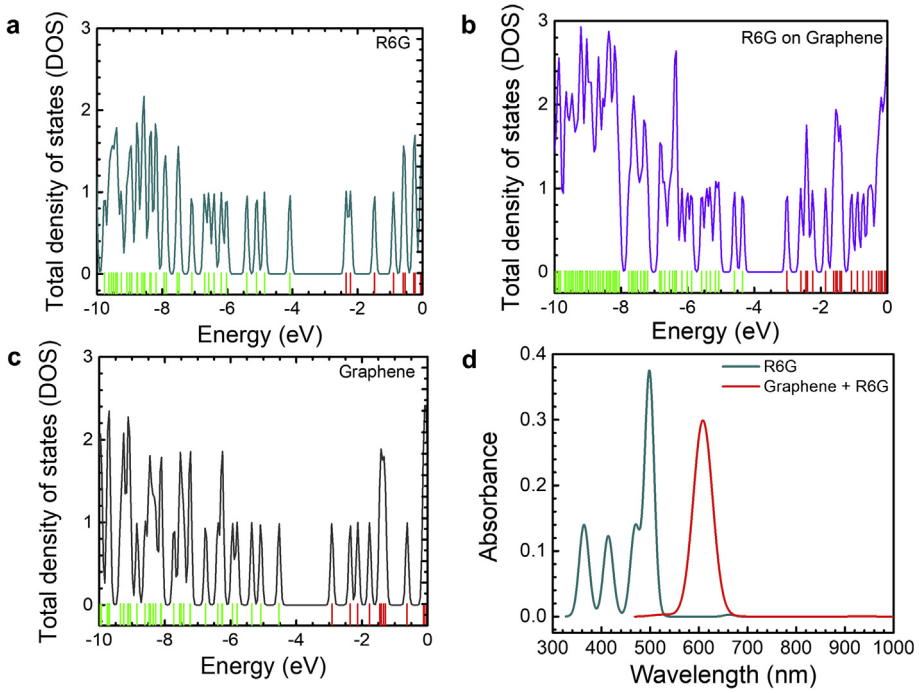

Fig. 9. Distribution of total density of states (DOS) for (a) R6G, (b) R6G on graphene, and (c) graphene showing the occupied (green) and unoccupied (red) molecular orbitals. The Fermi level is set as 0 eV. (d) Theoretical absorption spectrum (DFT) of R6G and R6G adsorbed on graphene. (A colour version of this figure can be viewed online.)

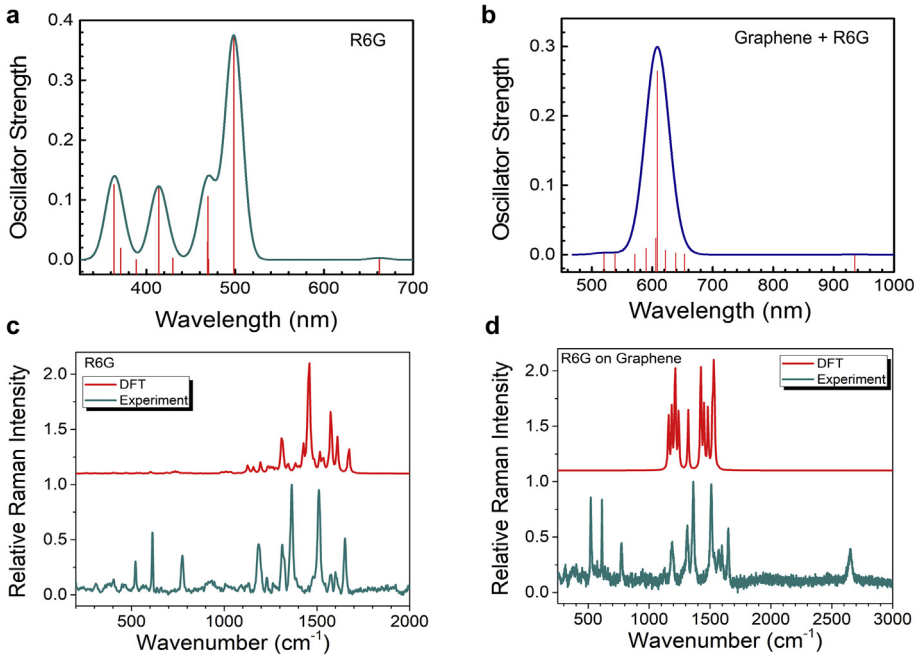

Fig. 10. (a) Absorption spectrum of R6G showing the strength of different singlet-singlet transitions corresponding to the absorption peaks. (b) Absorption spectrum of R6G adsorbed on graphene showing the strength of different singlet-singlet transitions corresponding to the absorption peaks. Comparison of experimental (dark cyan) and DFT calculated (red) Raman spectra of (c) R6G, and (d) R6G adsorbed on graphene. (A colour version of this figure can be viewed online.)

hybrid system, *i.e.* electrons are supplied to the system, confirming charge transfer from graphene-to-R6G. From the electron density plot, the excited state of the hybrid system (LUMO) also showed more electrons in graphene than in R6G, which might be transferred during relaxation process. These results collectively show that the charge transfer is from graphene to R6G, supporting our hypothesis on the enhancement properties of ripples of graphene and emphasizing its application as SERS substrate.

In the previous section, the electronic structures, the adsorption energies, the charge transfers, and the ground state structures of R6G and SLG were discussed. In order to understand the role of electronic states in CM enhancement, we also examined the total density of states (DOS). The results of this study may provide meaningful insights, such as: (1) the number of available states at

each energy level which might reflect the total number of allowed transitions [78], and (2) increased DOS would lead to increased scattering, and hence enhancement of the Raman signal [79]. Fig. 9 presents the distribution of DOS for R6G, R6G on graphene, and graphene. The green lines show the occupied states, while the red lines show the unoccupied molecular orbitals. Comparing Figs. 9a–c, it is evident that the DOS is increased for R6G on graphene compared to R6G or graphene individually, indicating higher probability of transition for Raman scattering (Fig. 9b). These results show that R6G adsorption on graphene broadens the bandgap of graphene indicating the likelihood of energy transfer from graphene-to-R6G, wherein graphene acts as an electron donor and R6G as an electron acceptor. From the DOS studies, it can be understood that the charge transfer will induce the polarizability of R6G molecules and thus result in the enhancement of Raman scattering [80]. The theoretical absorption spectra obtained from DFT for R6G and R6G adsorbed on graphene are presented in Fig. 9d. Intense peak at ~500 nm (blue line) was found for R6G. For R6G adsorbed on graphene, a peak at ~630 nm (red line) was found. A peak shift is observed after adsorption of R6G on graphene. As mentioned earlier, utilizing the 633 nm laser for Raman spectroscopy near this absorption spectrum would potentially take advantage of the resonant absorption leading to stronger SERS activity.

In spite of the basic understanding that the number of available states at each energy level reflects the total number of allowed electrons, the theoretical efforts to describe this distribution and detail the transition behavior have not been presented so far. In the present study, we investigated the oscillator strength qualitatively using absorption measurements to find the permissible transition. An oscillator strength of ~1 implies complete transition. The absorption spectra basically reflect the fact that Absorption = DOS × Oscillator strength [81].

The absorption spectrum of R6G seen in Fig. 10a had the highest absorption peak at 498.3 nm, with a highest oscillator strength of 0.37391 corresponding to singlet-singlet transition from HOMO-→LUMO (Table S4). Another peak was observed at 413.8 nm with oscillator strength of 0.1223 with singlet-singlet transition from HOMO-2→LUMO. Another prominent peak at 363.3 nm with oscillator strength of 0.12555 with singlet-singlet transition from HOMO→LUMO+3 was also observed. For R6G adsorbed on graphene, as shown in Fig. 10b, one absorption peak at 608.6 nm with oscillator strength of 0.26438 corresponding to singlet-singlet transition from HOMO-1→LUMO was observed (Table S5). Finally, we also extrapolated the Raman spectrum of R6G and R6G adsorbed on graphene both experimentally (dark cyan lines) and through DFT calculations (red lines). From Fig. 10c, it is seen that most of the major peaks are simulated well, with the exception that some minor peaks are missing. This difference is because the simulations were done at 0 K in the gaseous state, while the experiment was conducted at room temperature in solid state. These results further strengthen the applicability of the designed SLG as SERS substrate. Table S6 presents the electrical properties of R6G and R6G adsorbed on graphene. The dipole moment of the hybrid system (Graphene + R6G) is lowered compared to the isolated R6G because of charge supply from graphene-to-R6G molecules. Due to strong dipolar molecules like R6G, coupled with possible π-π stacking interaction with graphene, strong interaction between graphene and R6G occurs at the interface. This leads to increase in the polarizability and anisotropy in the polarizability which is responsible for increase in the Raman intensity after adsorption in the hybrid structure.

The current state-of-art suggests that several strategies have been applied to increase the oscillator strength in the UV and visible spectral range by designing plasmonic assisted devices for efficient absorption enhancement for photovoltaics applications [82–84]. In the current scenario, we believe that studies on understanding how substrate fabrication could improve the oscillator strength, could potentially help build better plasmonic assisted SERS substrates.

4. Conclusion

We investigated the enhancement properties of a rippled single layer of graphene deposited on a 3D Au@Ag core-shell nanopillar structure. We investigated the optical reflectance and scattering properties of the graphene covered SERS substrate. The presence of a SLG was confirmed by the FWHM of the G and 2D bands as well as the 2D to G peak ratio. We showed that the rippled structure of graphene splits the G peak into two peaks due to ripple-mediated strain on the graphene structure. The Raman spectra was acquired for R6G dye molecules adsorbed on the SLG/SERS substrate. The ripples on the graphene covered plasmonic SERS substrate led to more than 1000× higher SERS enhancement factor at 633 nm excitation laser for each identified Raman peak in comparison to the flat substrate under the same conditions. Concentration dependent studies of the SERS spectra of R6G on the graphene covered Au@Ag core-shell substrate showed a detection limit of 100 pM. The SERS substrate provided ~10^2–10^3 factor of enhancement in the cross-section of R6G ($\sigma_{R6G} = 0.27 - 1.62 \times 10^{-21}$ $cm^2 \cdot Sr^{-1}$) for the Raman scattering process. The FDTD simulations showed field intensity enhancement from plasmonic nanostructures due to localization of the field in the vicinity of the graphene monolayer, enhancing the optical absorption rate in graphene. The chemical enhancement *via* DFT calculations showed that the charge transfer from graphene to R6G molecule is responsible for the Raman scattering enhancement properties of rippled graphene. Strong interaction between graphene and R6G occurs at the interface because of the strong dipolar nature of R6G molecule along with molecular interaction due to π- π stacking interaction with graphene. As a result, the Raman intensity is enhanced due to the increase in the polarizability as well as the anisotropy from rippled graphene substrate.

Acknowledgements

We thank LSU Shared Instrumentation Facility and Dr. Dongmei Cao for the SEM images. M.R.G. thanks the support from LSU start-up fund, Louisiana Board of Regents Support Fund (RCS Award Contract Number: LEQSF(2017-20)-RD-A-04), and LaSPACE (LEQSF (2015-18)-LASPACE, GR-4216). A.P. was supported by the National Science Foundation (NSF Award Number:1660233). G.V. acknowledges support from the National Science Foundation (NSF Award Number:1254934). A.C. is supported by an LSU Economic Development Assistantship (EDA) grant.

Appendix A. Supplementary data

Supplementary data to this article can be found online at https://doi.org/10.1016/j.carbon.2019.09.078.

References

[1] Q. Hao, B. Wang, J.A. Bossard, B. Kiraly, Y. Zeng, I.-K. Chiang, L. Jensen, D.H. Werner, T.J. Huang, Surface-enhanced Raman scattering study on graphene-coated metallic nanostructure substrates, J. Phys. Chem. C 116 (13) (2012) 7249–7254.
[2] Y. Li, W. Shi, N. Chopra, Functionalization of multilayer carbon shell-encapsulated gold nanoparticles for surface-enhanced Raman scattering sensing and DNA immobilization, Carbon 100 (2016) 165–177.
[3] Y. Zhao, Y. Xie, Z. Bao, Y.H. Tsang, L. Xie, Y. Chai, Enhanced SERS stability of

R6G molecules with monolayer graphene, J. Phys. Chem. C 118 (22) (2014) 11827–11832.
[4] Y. Jiang, J. Wang, L. Malfatti, D. Carboni, N. Senes, P. Innocenzi, Highly durable graphene-mediated surface enhanced Raman scattering (G-SERS) nanocomposites for molecular detection, Appl. Surf. Sci. 450 (2018) 451–460.
[5] X. Xiu, Y. Guo, C. Li, Z. Li, D. Li, C. Zang, S. Jiang, A. Liu, B. Man, C. Zhang, High-performance 3D flexible SERS substrate based on graphene oxide/silver nanoparticles/pyramid PMMA, Opt. Mater. Express 8 (4) (2018) 844–857.
[6] A. Prasad, J. Choi, Z. Jia, S. Park, M.R. Gartia, Nanohole Array Plasmonic Biosensors: Emerging Point-Of-Care Applications, Biosensors and Bioelectronics, 2019.
[7] X. Kong, Q. Chen, The positive influence of boron-doped graphene with pyridine as a probe molecule on SERS: a density functional theory study, J. Mater. Chem. 22 (30) (2012) 15336–15341.
[8] Y. Wang, H. Chen, M. Sun, Z. Yao, B. Quan, Z. Liu, Y. Weng, J. Zhao, C. Gu, J. Li, Ultrafast carrier transfer evidencing graphene electromagnetically enhanced ultrasensitive SERS in graphene/Ag-nanoparticles hybrid, Carbon 122 (2017) 98–105.
[9] N. Yi, C. Zhang, Q. Song, S. Xiao, A hybrid system with highly enhanced graphene SERS for rapid and tag-free tumor cells detection, Sci. Rep. 6 (2016) 25134.
[10] S. Botti, A. Rufoloni, S. Laurenzi, S. Gay, T. Rindzevicius, M.S. Schmidt, M.G. Santonicola, DNA self-assembly on graphene surface studied by SERS mapping, Carbon 109 (2016) 363–372.
[11] S. Sharma, V. Prakash, S. Mehta, Graphene/silver nanocomposites-potential electron mediators for proliferation in electrochemical sensing and SERS activity, Trends Anal. Chem. 86 (2017) 155–171.
[12] L. Ouyang, Y. Hu, L. Zhu, G.J. Cheng, J. Irudayaraj, A reusable laser wrapped graphene-Ag array based SERS sensor for trace detection of genomic DNA methylation, Biosens. Bioelectron. 92 (2017) 755–762.
[13] X. Zhu, L. Shi, M.S. Schmidt, A. Boisen, O. Hansen, J. Zi, S. Xiao, N.A. Mortensen, Enhanced light–matter interactions in graphene-covered gold nanovoid arrays, Nano Lett. 13 (10) (2013) 4690–4696.
[14] Z. Osváth, A. Deák, K. Kertész, G. Molnár, G. Vértesy, D. Zámbó, C. Hwang, L.P. Biró, The structure and properties of graphene on gold nanoparticles, Nanoscale 7 (12) (2015) 5503–5509.
[15] Y. Zhang, S. Liu, L. Wang, X. Qin, J. Tian, W. Lu, G. Chang, X. Sun, One-pot green synthesis of Ag nanoparticles-graphene nanocomposites and their applications in SERS, H 2 O 2, and glucose sensing, RSC Adv. 2 (2) (2012) 538–545.
[16] X. Yu, H. Cai, W. Zhang, X. Li, N. Pan, Y. Luo, X. Wang, J. Hou, Tuning chemical enhancement of SERS by controlling the chemical reduction of graphene oxide nanosheets, ACS Nano 5 (2) (2011) 952–958.
[17] A.C. Ferrari, D.M. Basko, Raman spectroscopy as a versatile tool for studying the properties of graphene, Nat. Nanotechnol. 8 (4) (2013) 235.
[18] F. Schedin, E. Lidorikis, A. Lombardo, V.G. Kravets, A.K. Geim, A.N. Grigorenko, K.S. Novoselov, A.C. Ferrari, ACS Nano 4 (2010) 5617.
[19] A. Mahigir, T.-W. Chang, A. Behnam, G.L. Liu, M.R. Gartia, G. Veronis, Plasmonic nanohole array for enhancing the SERS signal of a single layer of graphene in water, Sci. Rep. 7 (1) (2017) 14044.
[20] L. Xie, X. Ling, Y. Fang, J. Zhang, Z. Liu, Graphene as a substrate to suppress fluorescence in resonance Raman spectroscopy, J. Am. Chem. Soc. 131 (29) (2009) 9890–9891.
[21] X. Ling, L. Xie, Y. Fang, H. Xu, H. Zhang, J. Kong, M.S. Dresselhaus, J. Zhang, Z. Liu, Can graphene be used as a substrate for Raman enhancement? Nano Lett. 10 (2) (2009) 553–561.
[22] J. Mertens, A.L. Eiden, D.O. Sigle, F. Huang, A. Lombardo, Z. Sun, R.S. Sundaram, A. Colli, C. Tserkezis, J. Aizpurua, Controlling subnanometer gaps in plasmonic dimers using graphene, Nano Lett. 13 (11) (2013) 5033–5038.
[23] G. Lu, H. Li, C. Liusman, Z. Yin, S. Wu, H. Zhang, Surface enhanced Raman scattering of Ag or Au nanoparticle-decorated reduced graphene oxide for detection of aromatic molecules, Chem. Sci. 2 (9) (2011) 1817–1821.
[24] W. Xu, X. Ling, J. Xiao, M.S. Dresselhaus, J. Kong, H. Xu, Z. Liu, J. Zhang, Surface enhanced Raman spectroscopy on a flat graphene surface, Proc. Natl. Acad. Sci. 109 (24) (2012) 9281–9286.
[25] M. Losurdo, I. Bergmair, B. Dastmalchi, T.H. Kim, M.M. Giangregroio, W. Jiao, G.V. Bianco, A.S. Brown, K. Hingerl, G. Bruno, Graphene as an electron shuttle for silver deoxidation: removing a key barrier to plasmonics and metamaterials for SERS in the visible, Adv. Funct. Mater. 24 (13) (2014) 1864–1878.
[26] K.J. Lee, D. Kim, B.C. Jang, D.J. Kim, H. Park, D.Y. Jung, W. Hong, T.K. Kim, Y.K. Choi, S.Y. Choi, Multilayer graphene with a rippled structure as a spacer for improving plasmonic coupling, Adv. Funct. Mater. 26 (28) (2016) 5093–5101.
[27] J. Leem, M.C. Wang, P. Kang, S. Nam, Mechanically self-assembled, three-dimensional graphene–gold hybrid nanostructures for advanced nanoplasmonic sensors, Nano Lett. 15 (11) (2015) 7684–7690.
[28] W. Xu, N. Mao, J. Zhang, Graphene: a platform for surface-enhanced Raman spectroscopy, Small 9 (8) (2013) 1206–1224.
[29] F. Schedin, E. Lidorikis, A. Lombardo, V.G. Kravets, A.K. Geim, A.N. Grigorenko, K.S. Novoselov, A.C. Ferrari, Surface-enhanced Raman spectroscopy of graphene, ACS Nano 4 (10) (2010) 5617–5626.
[30] P. Wang, O. Liang, W. Zhang, T. Schroeder, Y.H. Xie, Ultra-sensitive graphene-plasmonic hybrid platform for label-free detection, Adv. Mater. 25 (35) (2013) 4918–4924.
[31] L. Ju, B. Geng, J. Horng, C. Girit, M. Martin, Z. Hao, H.A. Bechtel, X. Liang, A. Zettl, Y.R. Shen, Graphene plasmonics for tunable terahertz metamaterials, Nat. Nanotechnol. 6 (10) (2011) 630.
[32] Y. Li, N. Chopra, Graphene encapsulated gold nanoparticle-quantum dot heterostructures and their electrochemical characterization, Appl. Surf. Sci. 344 (2015) 27–32.
[33] P. Tian, L. Tang, K.S. Teng, J. Xiang, S.P. Lau, Recent Advances in Graphene Homogeneous P–N Junction for Optoelectronics, Advanced Materials Technologies, 2019, p. 1900007.
[34] T. Deng, Z. Zhang, Y. Liu, Y. Wang, F. Su, S. Li, Y. Zhang, H. Li, H. Chen, Z. Zhao, Three-dimensional graphene field-effect transistors as high-performance photodetectors, Nano Lett. 19 (3) (2019) 1494–1503.
[35] A.C. Tasolamprou, A.D. Koulouklidis, C. Daskalaki, C.P. Mavidis, G. Kenanakis, G. Deligeorgis, Z. Viskadourakis, P. Kuzhir, S. Tzortzakis, M. Kafesaki, Experimental Demonstration of Ultrafast THz Modulation in a Graphene-Based Thin Film Absorber through Negative Photoinduced Conductivity, ACS photonics, 2019.
[36] Z. Sun, T. Hasan, F. Torrisi, D. Popa, G. Privitera, F. Wang, F. Bonaccorso, D.M. Basko, A.C. Ferrari, Graphene mode-locked ultrafast laser, ACS Nano 4 (2) (2010) 803–810.
[37] A.S. Rad, E. Sani, E. Binaeian, M. Peyravi, M. Jahanshahi, DFT study on the adsorption of diethyl, ethyl methyl, and dimethyl ethers on the surface of gallium doped graphene, Appl. Surf. Sci. 401 (2017) 156–161.
[38] M. Hinnemo, P. Ahlberg, C. Hägglund, W. Ren, H.-M. Cheng, S.-L. Zhang, Z.-B. Zhang, Scalable residue-free graphene for surface-enhanced Raman scattering, Carbon 98 (2016) 567–571.
[39] J. Kierdaszuk, P. Kaźmierczak, R. Bożek, J. Grzonka, A. Krajewska, Z.R. Zytkiewicz, M. Sobanska, K. Klosek, A. Wołoś, M. Kamińska, Surface-enhanced Raman scattering of graphene caused by self-induced nanogating by GaN nanowire array, Carbon 128 (2018) 70–77.
[40] Y. Li, J. Dykes, T. Gilliam, N. Chopra, A new heterostructured SERS substrate: free-standing silicon nanowires decorated with graphene-encapsulated gold nanoparticles, Nanoscale 9 (16) (2017) 5263–5272.
[41] M. Chapman, M. Mullen, E. Novoa-Ortega, M. Alhasani, J.F. Elman, W.B. Euler, Structural evolution of ultrathin films of rhodamine 6G on glass, J. Phys. Chem. C 120 (15) (2016) 8289–8297.
[42] A.V. Bobrov, Y.S. Marfin, V.V. Kuznetsov, E.V. Rumyantsev, Sol–gel synthesis, spectral properties and stability of silica films doped by fluorescent dyes, Mater. Technol. 32 (2) (2017) 116–123.
[43] R.C. Weast, M.J. Astle, W.H. Beyer, CRC Handbook of Chemistry and Physics, CRC press, Boca Raton, FL, 1988.
[44] M. Bruna, S. Borini, Optical constants of graphene layers in the visible range, Appl. Phys. Lett. 94 (3) (2009).
[45] R.R. Nair, P. Blake, A.N. Grigorenko, K.S. Novoselov, T.J. Booth, T. Stauber, N.M.R. Peres, A.K. Geim, Fine structure constant defines visual transparency of graphene, Science 320 (5881) (2008) 1308.
[46] A. Taflove, S.C. Hagness, Computational Electrodynamics, Artech house publishers2000.
[47] K. Zhang, S. Yu, B. Jv, W. Zheng, Interaction of Rhodamine 6G molecules with graphene: a combined computational–experimental study, Phys. Chem. Chem. Phys. 18 (41) (2016) 28418–28427.
[48] R.R. Nair, P. Blake, A.N. Grigorenko, K.S. Novoselov, T.J. Booth, T. Stauber, N.M. Peres, A.K. Geim, Fine structure constant defines visual transparency of graphene, Science 320 (5881) (2008), 1308-1308.
[49] Q. Liu, Y. Tian, W. Tang, X. Jing, J. Zhang, S. Xu, Comprehensive studies of the Ag^{+} effect on borosilicate glass ceramics containing Ag nanoparticles and Er-doped hexagonal $NaYF_4$ nanocrystals: morphology, structure, and 2.7 μm emission, Nanophotonics 7 (5) (2018) 913–923.
[50] A. Chaichi, A. Prasad, M. Gartia, Raman spectroscopy and microscopy applications in cardiovascular diseases: from molecules to organs, Biosensors 8 (4) (2018) 107.
[51] P. Senanayake, C.-H. Hung, J. Shapiro, A. Lin, B. Liang, B.S. Williams, D. Huffaker, Surface plasmon-enhanced nanopillar photodetectors, Nano Lett. 11 (12) (2011) 5279–5283.
[52] K. Kertész, A. Koós, A. Murdock, Z. Vértesy, P. Nemes-Incze, P. Szabó, Z. Horváth, L. Tapasztó, C. Hwang, N. Grobert, Polarized light microscopy of chemical-vapor-deposition-grown graphene on copper, Appl. Phys. Lett. 100 (21) (2012) 213103.
[53] W. Zhao, M. Fang, F. Wu, H. Wu, L. Wang, G. Chen, Preparation of graphene by exfoliation of graphite using wet ball milling, J. Mater. Chem. 20 (28) (2010) 5817–5819.
[54] M. Lazzeri, F. Mauri, Nonadiabatic Kohn anomaly in a doped graphene monolayer, Phys. Rev. Lett. 97 (26) (2006) 266407.
[55] A. Das, B. Chakraborty, A. Sood, Raman spectroscopy of graphene on different substrates and influence of defects, Bull. Mater. Sci. 31 (3) (2008) 579–584.
[56] Z. Lin, X. Ye, J. Han, Q. Chen, P. Fan, H. Zhang, D. Xie, H. Zhu, M. Zhong, Precise control of the number of layers of graphene by picosecond laser thinning, Sci. Rep. 5 (2015) 11662.
[57] Y. Hao, Y. Wang, L. Wang, Z. Ni, Z. Wang, R. Wang, C.K. Koo, Z. Shen, J.T. Thong, Probing layer number and stacking order of few-layer graphene by Raman spectroscopy, Small 6 (2) (2010) 195–200.
[58] C. Li, D. Li, J. Yang, X. Zeng, W. Yuan, Preparation of single-and few-layer graphene sheets using co deposition on SiC substrate, J. Nanomater. 2011 (2011) 44.
[59] G.S. Petreska, J. Blazevska-Gilev, R. Fajgar, R. Tomovska, Surface-Enhanced Raman Scattering activity of Ag/graphene/polymer nanocomposite films

synthesized by laser ablation, Thin Solid Films 564 (2014) 115–120.
[60] X.N. He, Y. Gao, M. Mahjouri-Samani, P.N. Black, J. Allen, M. Mitchell, W. Xiong, Y. Zhou, L. Jiang, Y. Lu, Surface-enhanced Raman spectroscopy using gold-coated horizontally aligned carbon nanotubes, Nanotechnology 23 (20) (2012) 205702.
[61] E.S. Thrall, A.C. Crowther, Z. Yu, L.E. Brus, R6G on graphene: high Raman detection sensitivity, yet decreased Raman cross-section, Nano Lett. 12 (3) (2012) 1571–1577.
[62] M.R. Kagan, R.L. McCreery, Quantitative surface Raman spectroscopy of physisorbed monolayers on glassy carbon, Langmuir 11 (10) (1995) 4041–4047.
[63] N. Wada, S. Solin, Raman efficiency measurements of graphite, Phys. B+C 105 (1–3) (1981) 353–356.
[64] S. Shim, C.M. Stuart, R.A. Mathies, Resonance Raman cross-sections and vibronic analysis of rhodamine 6G from broadband stimulated Raman spectroscopy, ChemPhysChem 9 (5) (2008) 697–699.
[65] S. Heeg, R. Fernandez-Garcia, A. Oikonomou, F. Schedin, R. Narula, S.A. Maier, A. Vijayaraghavan, S. Reich, Polarized plasmonic enhancement by Au nanostructures probed through Raman scattering of suspended graphene, Nano Lett. 13 (1) (2012) 301–308.
[66] T. Mohiuddin, A. Lombardo, R. Nair, A. Bonetti, G. Savini, R. Jalil, N. Bonini, D. Basko, C. Galiotis, N. Marzari, Uniaxial strain in graphene by Raman spectroscopy: G peak splitting, Grüneisen parameters, and sample orientation, Phys. Rev. B 79 (20) (2009) 205433.
[67] X. Zheng, W. Chen, G. Wang, Y. Yu, S. Qin, J. Fang, F. Wang, X.-A. Zhang, The Raman redshift of graphene impacted by gold nanoparticles, AIP Adv. 5 (5) (2015), 057133.
[68] R. Goul, S. Das, Q. Liu, M. Xin, R. Lu, R. Hui, J.Z. Wu, Quantitative analysis of surface enhanced Raman spectroscopy of Rhodamine 6G using a composite graphene and plasmonic Au nanoparticle substrate, Carbon 111 (2017) 386–392.
[69] X. Li, W.C. Choy, X. Ren, D. Zhang, H. Lu, Highly intensified surface enhanced Raman scattering by using monolayer graphene as the nanospacer of metal film–metal nanoparticle coupling system, Adv. Funct. Mater. 24 (21) (2014) 3114–3122.
[70] X. Ling, L. Moura, M.A. Pimenta, J. Zhang, Charge-transfer mechanism in graphene-enhanced Raman scattering, J. Phys. Chem. C 116 (47) (2012) 25112–25118.
[71] X. Zhao, M. Chen, Charge transfer mechanism of SERS for metal–molecule–metal junction supported by graphene and boron-doped graphene, RSC Adv. 4 (108) (2014) 63596–63602.
[72] C. Huang, M. Kim, B.M. Wong, N.S. Safron, M.S. Arnold, P. Gopalan, Raman enhancement of a dipolar molecule on graphene, J. Phys. Chem. C 118 (4) (2014) 2077–2084.
[73] S. Banerjee, M. Sardar, N. Gayathri, A. Tyagi, B. Raj, Conductivity landscape of highly oriented pyrolytic graphite surfaces containing ribbons and edges, Phys. Rev. B 72 (7) (2005), 075418.
[74] S. Banerjee, M. Sardar, N. Gayathri, A. Tyagi, B. Raj, Enhanced conductivity in graphene layers and at their edges, Appl. Phys. Lett. 88 (6) (2006), 062111.
[75] Y. Niimi, T. Matsui, H. Kambara, K. Tagami, M. Tsukada, H. Fukuyama, Scanning tunneling microscopy and spectroscopy of the electronic local density of states of graphite surfaces near monoatomic step edges, Phys. Rev. B 73 (8) (2006), 085421.
[76] B. Obradovic, R. Kotlyar, F. Heinz, P. Matagne, T. Rakshit, M. Giles, M. Stettler, D. Nikonov, Analysis of graphene nanoribbons as a channel material for field-effect transistors, Appl. Phys. Lett. 88 (14) (2006) 142102.
[77] L. Yang, M.L. Cohen, S.G. Louie, Excitonic effects in the optical spectra of graphene nanoribbons, Nano Lett. 7 (10) (2007) 3112–3115.
[78] M. Amft, B. Sanyal, O. Eriksson, N.V. Skorodumova, Small gold clusters on graphene, their mobility and clustering: a DFT study, J. Phys. Condens. Matter 23 (20) (2011) 205301.
[79] H.-p. Zhang, X.-g. Luo, X.-y. Lin, X. Lu, Y. Leng, H.-t. Song, Density functional theory calculations on the adsorption of formaldehyde and other harmful gases on pure, Ti-doped, or N-doped graphene sheets, Appl. Surf. Sci. 283 (2013) 559–565.
[80] J. Shang, L. Ma, J. Li, W. Ai, T. Yu, G.G. Gurzadyan, The origin of fluorescence from graphene oxide, Sci. Rep. 2 (2012) 792.
[81] M. Bednarz, V. Malyshev, J. Knoester, Low-temperature dynamics of weakly localized Frenkel excitons in disordered linear chains, J. Chem. Phys. 120 (8) (2004) 3827–3840.
[82] C. Hägglund, S.P. Apell, B. Kasemo, Maximized optical absorption in ultrathin films and its application to plasmon-based two-dimensional photovoltaics, Nano Lett. 10 (8) (2010) 3135–3141.
[83] Q. Gu, Plasmonic metallic nanostructures for efficient absorption enhancement in ultrathin CdTe-based photovoltaic cells, J. Phys. D 43 (46) (2010) 465101.
[84] C. Hägglund, G. Zeltzer, R. Ruiz, I. Thomann, H.-B.-R. Lee, M.L. Brongersma, S.F. Bent, Self-assembly based plasmonic arrays tuned by atomic layer deposition for extreme visible light absorption, Nano Lett. 13 (7) (2013) 3352–3357.